Design of new cold rolled purlins by experimental testing and Direct Strength Method

V.B. Nguyen[a,*], C.H. Pham[b], B. Cartwright[c] and M.A. English[c]

[a]*Lecturer, Department of Civil Engineering, College of Engineering and Technology, University of Derby, Markeaton Street, Derby, DE22 3AW, United Kingdom*

[b]*Lecturer in Structural Engineering, School of Civil Engineering, Faculty of Engineering and Information Technologies, The University of Sydney, NSW 2006, Australia*

[c]*Product Development Manager, Hadley Industries plc, Smethwick, West Midlands, United Kingdom*

[c]*Design and Development Manager, Hadley Industries plc, Smethwick, West Midlands, United Kingdom*

[*] Corresponding author.

Tel: +44 (0) 1332 593587.

Email address: vb.nguyen@derby.ac.uk (V.B. Nguyen)

Keywords: Cold-formed, channel section, zed section, buckling strength, four-point bending test, Finite Element analysis, Direct Strength Method

Abstract

New cold roll formed channel and zed sections for purlins, namely UltraBEAM^{TM}2 and UltraZED^{TM}2, have been developed by Hadley Industries plc using a combined approach of experimental testing, finite element modelling and optimisation techniques. The new sections have improved strength to weight ratio by increasing the section's strength through the use of stiffeners in the section webs. The European standard, Eurocode 3 [1], uses the traditional Effective Width Method to determine the strength of a cold formed steel member. However, the design of the new sections UltraBEAM^{TM}2 and UltraZED^{TM}2 using this method is very complicated in calculating the effective section properties as these sections contain complex folded-in stiffeners. In addition, the incorporation of competing buckling modes such as distortional buckling of these sections can be difficult to analyse. To overcome difficulties of using Eurocode 3 or such a standard with the Effective Width Method for determining the strength of these sections, the Direct Strength Method is adopted in this paper. Four-point beam bending tests were carried out to determine the buckling and ultimate bending capacities of the UltraBEAM^{TM}2 and UltraZED^{TM}2 sections. Results from both experimental testing and Finite Element analysis were initially used as validation for the design using the Direct Strength Method. The Direct Strength Method's results were then compared with the experimental test results for a broader data in which the UltraBEAM^{TM}2 and UltraZED^{TM}2 sections had a range of different width-to-thickness ratios. It showed an excellent agreement between test and Direct Strength design values suggesting that the Direct Strength Method is a powerful tool for the design and optimisation of the new cold roll formed channel and zed purlins.

1. Introduction

Cold-formed purlin sections are usually manufactured into conventional channel and zed profiles. These sections consist of plate elements of the web and flanges which usually have a large width-to-thickness ratio. Therefore, they are prone to local or distortional buckling and these buckling phenomena govern the failure modes for cold-formed steel members. There have been extensive investigations on buckling and ultimate strengths of these conventional sections. Practical design methods for these sections are normally specified in codes of practice in different countries such as European Standard [1], North American Specification [2,3] and Australian/New Zealand Standard [4].

To improve the strength of cold-formed sections that are prone to local and distortional buckling, stiffeners have been placed at the web of the sections. These stiffeners subdivide the plate elements into smaller sub-elements and hence can considerably increase the local buckling of cold-formed sections subjected to compressive stresses due to the smaller width-to-thickness ratio of the sub-elements. In recent years, there has been a significant number of studies on the strength and design of cold-formed sections with web stiffeners [5-9]. However, the majority of these studies are for columns under compression or hat sections under bending and there have been limited investigations on channel and zed sections with web stiffeners subjected to bending.

A zed section with longitudinal stiffeners in the web, introduced during the cold roll forming, was designed and developed at the University of Strathclyde by Rhodes and Zaras [10] in conjunction with Hadley Industries plc, with the aim of improving the performance of a zed type

section. The development using an analytical method suggested that when the stiffeners were placed about one fifth of the web width from each flange, the problem of local buckling in the web was eliminated. The channel section with longitudinal stiffeners in the web was later developed at Hadley Industries plc in an attempt to incorporate the innovative web stiffener configuration used in the new zed, into a channel shape [11]. Recent investigations using Finite Element analysis (FEA) and optimisation techniques have proved that when the two symmetrical stiffeners on the web were placed as much closely as possible to each flange, maximum buckling and ultimate strengths for the section were achieved [12,23]. Since the sections evolved had the basic zed shape, Z, and channel shape, C, with additional enhancements which proved improved performance, it was decided that these sections should be named the 'UltraZED^{TM}2' and 'UltraBEAM^{TM}2' as illustrated in Fig. 1, respectively from now on in this paper. The purlins developed are now registered designs, with patents applied for.

These new sections have a considerably improved strength to weight ratio considerably by using the web stiffener types as shown in Fig. 1. Additional small stiffeners in zed sections that have large width-to-thickness ratios were added to introduce a greater degree of work hardening, which raises the material yield strength in these regions, taking increased further advantage of eliminating the local and distortional buckling. All of the current design codes including the European standard Eurocode 3 (EC3) use the traditional Effective Width Method (EWM) to determine the strength of a cold formed steel member. However, the design of the new sections UltraBEAM^{TM}2 and UltraZED^{TM}2 using this method is very complicated and impractical in calculating the effective section properties as these sections contain complex folded-in stiffeners.

In addition, the incorporation of competing buckling modes such as distortional buckling can be difficult for these sections.

An alternative to the EWM is the newly developed Direct Strength Method (DSM) [13] which was first formally adopted in the North American Specification in 2004 [3] and Australian/New Zealand standard [4]. In development of the DSM for beam bending, two series of flexural tests and finite element analyses on both plain channel and zed sections were conducted to isolate local buckling [14] and distortional buckling [15]. Additional tests on distortional buckling have also been conducted by Javaroni and Goncalves [16]. Recently, Pham and Hancock [17] provided additional experimental data on both plain C- and SupaCee channel sections in pure bending. In their study, the SupaCee purlin profile is a complex section with four small longitudinal web stiffeners and return lips which was developed by BlueScope Lysaght (BlueScope Steel Ltd., Melbourne, Australia) and the University of Sydney (Sydney, Australia). They found that the local and distortional buckling test results are better predicted by the DSM curves for slender sections.

The DSM uses the elastic buckling loads for the gross section considering local, distortional and global buckling to determine the strength of a cold-formed steel member. The DSM does not need to calculate the effective section properties; instead the elastic buckling analysis is calculated with computer aided numerical analysis so it can be used for design of cold-formed steel members with complex stiffeners [18]. On the other hand, the DSM in current specifications is a semi-empirical approach, which was calibrated to cover only the pre-qualified sections specified in NAS [2,3]. Unfortunately, sections with complex longitudinal stiffeners like

the UltraBEAM™2 and UltraZED™2 shapes are not in lists of pre-qualified sections for using the DSM in any current design specifications. Therefore, the DSM was adopted in this paper for design of the UltraBEAM™2 and UltraZED™2 purlins and it was evaluated against experimental tests.

In this paper, four-point beam bending tests have been carried out to determine the ultimate bending capacity of the UltraBEAM™2 and UltraZED™2 sections which have a range of different geometries. Together with beam bending tests, tensile tests of the beam material were also conducted to determine the material properties. Finite Element (FE) simulations of the bending tests of the UltraBEAM™2 and UltraZED™2 sections were presented. The DSM in current specifications was evaluated for the strength of the UltraBEAM™2 and UltraZED™2 sections based on the experimental and FE results. The ultimate purpose of this study is to evaluate the applicability of the current Direct Strength Method for these new sections.

2. Experimental test programme

The beam specimens were cold roll formed along the rolling direction on steel coils with a nominal Young's modulus of 205 GPa. Typical cross sections of the test specimens are shown in Fig. 1. Measured test section geometries and dimensions are given in Table 1 for UltraBEAM™2 sections and Table 2 for UltraZED™2 sections. Dimensional measurements were carried out and recorded for all test specimens prior to testing. This allows the exact profile geometry to be evaluated within the DSM and FE simulations. Measurements taken include material thickness, web width (or depth), flange width, and lip length.

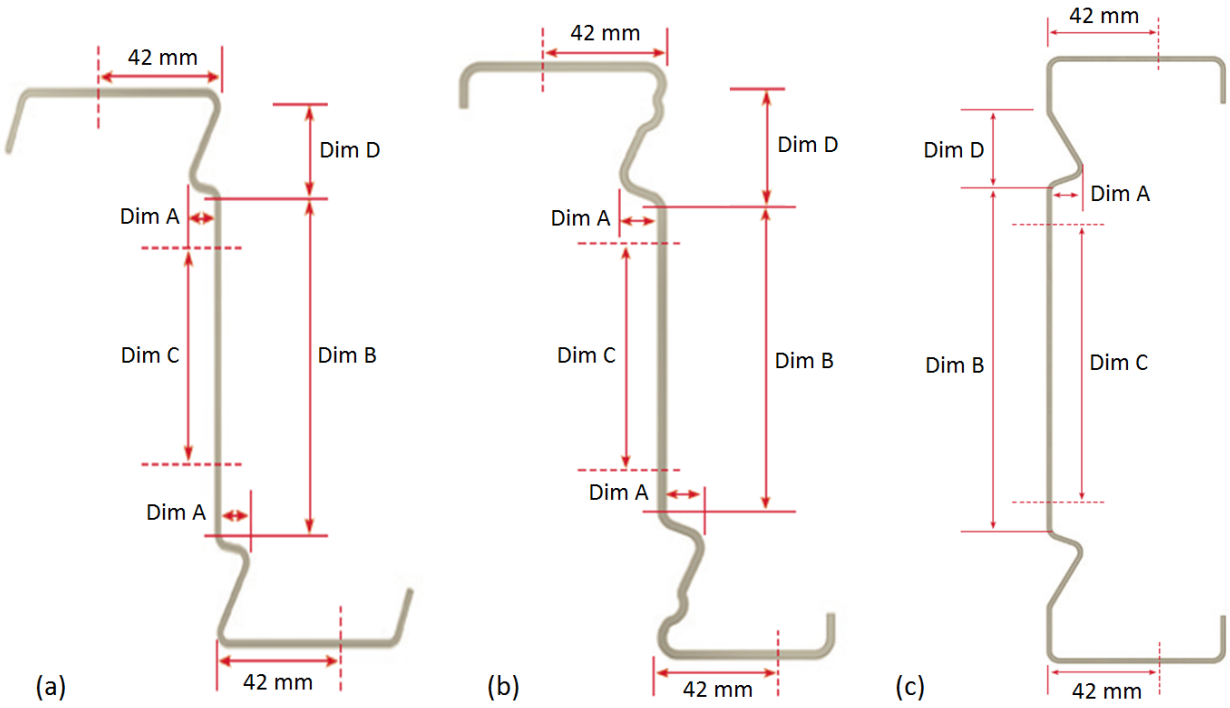

Fig. 1. Cross sections and geometries of beam specimens (a) UltraZED™2 145-170 mm deep sections, (b) UltraZED™2 200-305 mm deep sections, and (c) UltraBEAM™2 145-305 mm deep sections. The depth of the section is also called the web width; Dim C is the hole centre at the loading and end support positions

The beam specimens were labelled, an UltraBEAM™2 specimen label starts with C whilst an UltraZED™2 specimen starts with Z. For example, a specimen labelled as C-W145T1.2 is described as follows: C: Channel UltraBEAM™2 specimen; W: Web, 145: Nominal web height or beam depth (mm); T: Thickness, 1.2: Nominal plate thickness (mm). The forming process of each specimen is cold-rolled forming.

The material properties of the beam specimens were determined from tensile tests, adhering to Annex B of BS EN 10002-1:2001 [19]. Tensile test results in terms of yield stress, tensile strength and elongation are shown in Tables 1 and 2 for UltraBEAM^{TM}2 and UltraZED^{TM}2 steel materials, respectively. Experimental tests complying with standard BS EN 1993-1-3:2006 [1] were carried out to evaluate the FE and DSM results. A typical test setup for the four-point bending test of is shown in Fig. 2.

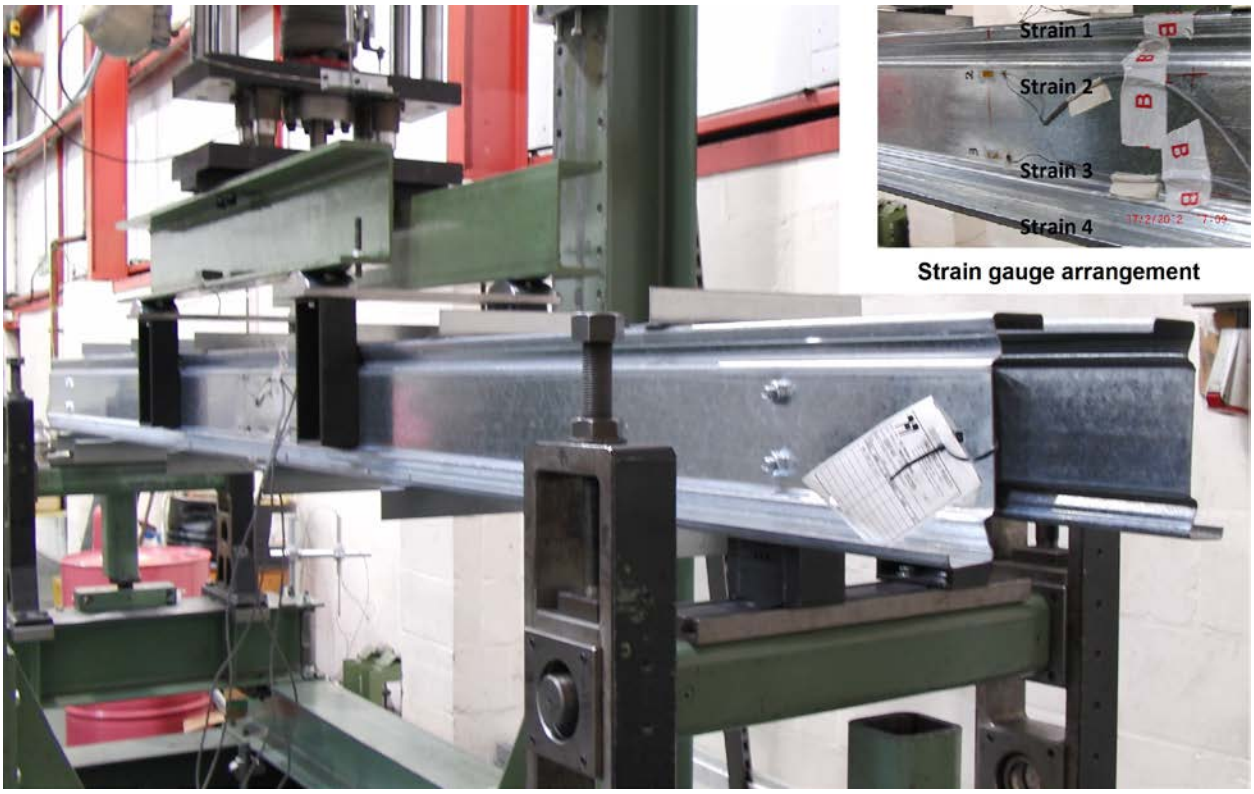

Fig. 2. Four-point bending test setup, showing UltraZED^{TM}2 sections and strain gauge arrangement (in box)

Table 1 Measured test section geometries and dimensions for UltraBEAM^{TM}2 sections

Channel sections				Flange		Dim A	Dim D	Dim B	Second Moment	Section modulus	Tensile Test Material Properties		
Section Reference	Thickness mm	Depth mm	Radius mm	Width mm	Lip mm	mm	mm	mm	Major axis mm^4x10^4	Major axis mm^3x10^3	Yield Stress N/mm^2	Tensile Strength N/mm^2	Elongation %
C-W145T1.2	1.23	145.04	2.30	63.07	16.05	9.00	20.00	75.00	121.54	16.76	485.50	530.00	14.00
C-W145T1.4	1.40	145.02	2.10	62.98	16.01	9.00	20.00	75.00	141.10	19.46	485.50	530.00	14.00
C-W145T2.0	1.99	145.01	1.50	63.05	16.01	9.00	20.00	75.00	198.64	27.40	485.10	515.00	15.00
C-W170T1.2	1.20	170.05	2.30	63.01	16.05	9.00	20.00	100.00	176.09	20.72	604.00	684.00	12.50
C-W170T1.5	1.50	169.80	2.00	62.99	15.94	9.00	20.00	100.00	218.66	25.72	557.00	575.00	14.00
C-W170T1.6	1.60	170.10	2.00	63.10	16.05	9.00	20.00	100.00	232.27	27.31	520.00	550.00	12.00
C-W170T2.0	2.01	170.00	1.50	63.04	15.98	9.00	20.00	100.00	288.34	33.92	535.00	640.00	14.00
C-W255T1.4	1.40	254.90	3.00	75.00	19.03	12.50	30.00	155.00	742.64	58.25	431.70	466.50	12.00
C-W255T2.3	2.32	255.02	2.10	75.06	19.02	12.50	30.00	155.00	820.21	64.33	450.20	545.00	26.00
C-W255T3.0	2.98	255.01	1.40	74.97	19.07	12.50	30.00	155.00	1009.89	79.21	487.00	552.00	27.00

Table 2 Measured test section geometries and dimensions for UltraZED^{TM}2 sections. The terms 'Flange Width' and 'Flange Lip' are full widths.

Zed Sections				Top flange		Bottom flange		Dim A	Dim D	Dim B	Second moment	Section modulus	Tensile test material properties		
Section Reference	Thickness mm	Depth mm	Radius mm	Width mm	Lip mm	Width mm	Lip mm	mm	mm	mm	Major axis mm^4x10^4	Major axis mm^3x10^3	Yield Stress N/mm^2	Tensile Strength N/mm^2	Elongation %
Z-W145T1.2	1.25	145.07	2.70	67.00	15.02	61.03	13.89	10.00	25.00	90.00	126.95	17.18	433.50	519.00	22.00
Z-W145T1.5	1.55	145.01	2.60	67.04	15.03	61.00	13.92	10.00	25.00	90.00	157.43	21.29	462.90	566.00	21.00
Z-W145T2.0	2.00	145.00	2.30	66.95	15.05	60.96	13.94	10.00	25.00	90.00	207.14	28.02	483.00	591.00	17.00
Z-W170T1.6	1.60	170.00	2.00	69.08	14.98	61.01	13.40	10.00	25.00	115.00	240.40	28.28	520.00	550.00	12.00
Z-W200T1.2	1.22	199.70	5.40	70.03	14.92	60.08	13.05	15.00	42.50	100.00	257.32	25.06	599.00	609.00	12.00
Z-W200T1.8	1.77	200.03	5.10	70.01	15.05	59.97	13.07	15.00	42.50	100.00	382.70	37.26	543.00	568.00	13.25
Z-W200T2.5	2.42	200.06	4.75	69.40	15.04	60.02	12.92	15.00	42.50	100.00	522.47	50.86	460.20	512.00	12.00
Z-W255T1.3	1.28	255.00	5.35	69.70	14.97	59.91	13.00	13.00	42.50	155.00	500.84	38.38	475.80	587.00	20.50
Z-W255T1.8	1.82	255.02	5.10	70.06	14.91	59.96	13.04	13.00	42.50	155.00	689.19	52.58	490.00	580.00	20.00
Z-W255T2.5	2.47	254.80	4.75	70.02	15.02	60.01	12.95	13.00	42.50	155.00	938.99	71.93	513.00	590.00	21.00

A calibrated test rig was used for the tests. The rig consists of a 220-kN capacity load cell (LCHD-50K model, Omega Engineering Ltd.) and an electric machine screw jack. The beams were set up as simply supported beams. Rotating end station, as shown in Fig. 2, was used to model the pin end condition of the beams at supports. Electrical strain gauges (SGD-10/120-LY11, Omega Engineering Ltd.) were used to measure the axial strains along the web and flanges of the cross section of the beam specimens; the critical buckling load was determined from strain gauge readings. Four strain gauges were mounted on the specimen mid-span, on the perimeter outside the specimen cross section, at the web positions close to the flanges and at the centres of flanges. LVDTs or displacement transducers were used for determining the vertical displacements from top and bottom of the beam specimens using the measurement procedure described in [20]. Each test consists of two opposing sections (UltraBEAM^{TM}2 sections had their flanges faced inwards whilst UltraZED^{TM}2 sections had their top flanges faced inwards), allowing application of load through or close to the shear centre of each section.

The load cell moved vertically down to apply a downward load symmetrically at two points at 0.33 x span centre. These loads were applied through the web of the section via a bolted connection using cleats (fixed to the beam webs), which in turn contacted the load cell beams via half round blocks, as shown in Fig. 2. The load was spread to the beams via this cleat system. Half round blocks were used to ensure that the load applied to cleats was a point load. In this testing arrangement, pure in-plane bending of the beams could be obtained between the two loading points without the presence of shear and axial force. Dedicated cleat components allowed end connection rotation through supporting stations, and defined load point application at the centres of the beams.

Test spans adhere to the minimum requirements as stated in the standard [1]. This distance was selected such that the ultimate load causing failure in the moment span is lower than that causing failure in the shear span. For accuracy during setting up, the beams were pierced during manufacture to allow fixing with M12 bolts (representative of those used in practice). The tested and manufactured spans are shown in Table 3. lateral restraints made of 45x45 mm steel angles were fixed by self-tapping screws to the top and bottom flanges at every 300-400 mm symmetrical to the mid-span and thereafter depending on beam depth and in turn the location of load points.

Table 3 Sample spans considered for testing and analysis

Section depth (mm)	145	170	200	225	255	305
Span (mm)	2295	2691	3087	3483	3879	4275
Load centre (mm)	765	897	1029	1161	1293	1425

Prior to each test the beam specimens were pre-loaded to remove any clearance in the connections, checking the alignment between specimens, connections and load cell. The applied load then returned to zero and the LVDTs and strain gauge readings were also set to zero. The specimens were loaded via the electric screw jack where displacement control was adopted to drive the load cell actuator at a constant rate of 2.5 mm/min. The specimens were loaded to failure and the test stopped at about 90% of the ultimate load. The data associated with load, displacement and strain gauge readings were recorded by the DASYLab data acquisition software (DASYLab software, Measurement Computing Corporation). Based on these data,

load-deflection curves were plotted. To take into account the variation in sample and testing conditions, 4 duplicated tests were carried out for each section referenced. There were 116 tests in total for both UltraBEAM^{TM}2 and UltraZED^{TM}2 beams.

3. Direct Strength Method

The Direct Strength Method specified in the North American Specification [2,3] was used in this study to determine the bending moment capacities of the UltraBEAM^{TM}2 and UltraZED^{TM}2 beams. This method considered elastic buckling loads identified from a numerical analysis. In particular, the finite strip software CUFSM [21,22] was used to identify the elastic buckling values for the beams. The elastic buckling analysis in CUFSM was performed for systematically increasing half-wavelengths to obtain the shapes and load factors for the buckling modes of the beam. Due to lateral restraints to the top and bottom flanges at every distance of 300-400 mm, no lateral-torsional buckling occurred to the beams in tests, so the beams were regarded as fully braced beams. Hence, the nominal flexural strength (M_{ne}) for lateral-torsional buckling was taken as the yield moment (M_y) for fully braced beams. The current DSM for beams that considered inelastic reserve capacities for local buckling and distortional buckling in the North American Specification were summarised as follows.

The ultimate flexural strength, M_n, is the minimum of nominal flexural strength due to global buckling (M_{ne}), nominal flexural strength for local buckling (M_{nl}) and nominal flexural strength for distortional buckling (M_{nd}), as shown as

$$M_n = \min(M_{ne}, M_{nl}, M_{nd}) \quad (1)$$

The nominal flexural strength for local buckling (M_{nl}) was calculated in accordance with the following:

For $\lambda_l \leq 0.776$, $M_{nl} = M_y$ (2)

For $\lambda_l > 0.776$, $M_{nl} = [1-0.15(M_{crl}/M_y)^{0.4}](M_{crl}/M_y)^{0.4}M_y$ (3)

Where $\lambda_l = (M_y/M_{crl})^{1/2}$; $M_y = S_f f_y$; S_f is the gross section modulus referenced to the extreme fiber at first yield; f_y is the yield stress which is the 0.2% proof stress ($\sigma_{0.2}$) obtained from tensile coupon tests in this study; M_{crl} is the critical elastic local buckling moment ($M_{crl} = S_f\sigma_{crl}$, in which σ_{crl} is the critical elastic local buckling stress).

The nominal flexural strength for distortional buckling (M_{nd}) was calculated in accordance with the following:

For $\lambda_d \leq 0.673$, $M_{nd} = M_y$ (4)

For $\lambda_d > 0.673$, $M_{nd} = [1-0.22(M_{crd}/M_y)^{0.5}](M_{crd}/M_y)^{0.5}M_y$ (5)

Where $\lambda_d = (M_y/M_{crd})^{1/2}$; M_{crd} is the critical elastic distortional buckling moment ($M_{crd} = S_f\sigma_{crd}$, in which σ_{crd} is the critical elastic distortional buckling stress).

The critical elastic local buckling stress σ_{crl}, critical elastic distortional buckling stress σ_{crd} and their half-wave lengths were obtained from the finite strip software CUFSM. As lateral restraints were attached at every 300 mm to 400 mm, which was smaller than the critical distortional buckling half-wave length in some the tests, they provided some restraint to the rotation of the compression flange and therefore limited the distortional buckling. In this study, the effects of

restraints were included in the calculation by using the distance between discrete restraints that limited the distortional buckling. Therefore, the elastic distortional buckling stress was calculated at the length between the two adjacent restraints. This stress value replaced the critical distortional buckling stress a in Eqn. (5). For example, in the test of Specimen C-W170T1.6, lateral restraints were attached by self-tapping screws at every 400mm and the elastic buckling stress was obtained at this length whilst the half-wave length for distortional buckling was 533.4 mm as shown in Fig. 4. In addition, tests with reduced distance between discrete restraints from 300 mm to 150 mm were carried out to see the effect of distance of restraints on buckling (results not shown); it was observed that only when the restraint distance of 150 mm the distortional buckling was completely prevented and local buckling occurred. Nevertheless, if the consistency of results could be obtained it could seem to further justify the assumption about obtaining elastic distortional buckling stress at the distance between two discrete restraints. The measured cross-section dimensions and material properties presented in Tables 1 and 2 were used to determine the theoretical buckling load.

4. Finite Element Analysis

Finite Element simulations were conducted using Marc (MSC Software, version 2015) to simulate the four-point bending test of the beams. In this example, the UltraBEAM^{TM}2 specimens **C-W170T1.6** had a total length of 2920 mm, a span of 2691 mm, a load centre of 897 mm, thickness of 1.60 mm, flange width of 63 mm, web width of 170 mm, lip length of 16 mm and corner radius of 2.0 mm. The UltraZED^{TM}2 specimens **Z-W170T1.6** had a total length of 2920 mm, a span of 2691 mm, a load centre of 897 mm, thickness of 1.60 mm, flange widths of

69 mm (top flange) and 61 mm (bottom flange), web width of 170 mm, lip length of 15 mm and corner radius of 2.0 mm. Other beam specimens had dimensions and material properties as presented in Table 1. Fig. 3 illustrates the FE model setup for the UltraBEAM^{TM}2. By taking advantage of symmetry, only a half of the test system was modelled. The beams were presented by shell elements on its central plane with a thickness of 1.60 mm. In these simulations, the material properties of the sheet steel were obtained from physical tensile tests. The braces were modelled as rigid links connections. Load was applied on the two central cleats at their centroids using the displacement-controlled method while the two end supports were fully fixed in vertical direction at their centroids. Each loading point was at a reference node that connects to a set of tied nodes (at the beam web where the cleat connected to the beam). The link between the reference node and the tied nodes was based on a rigid link connection, only unrestrained in loading direction. The displacement was increased in successive increments until the column failed. A full Newton-Raphson method was used for the iterative procedure and an implicit, static analysis was employed.

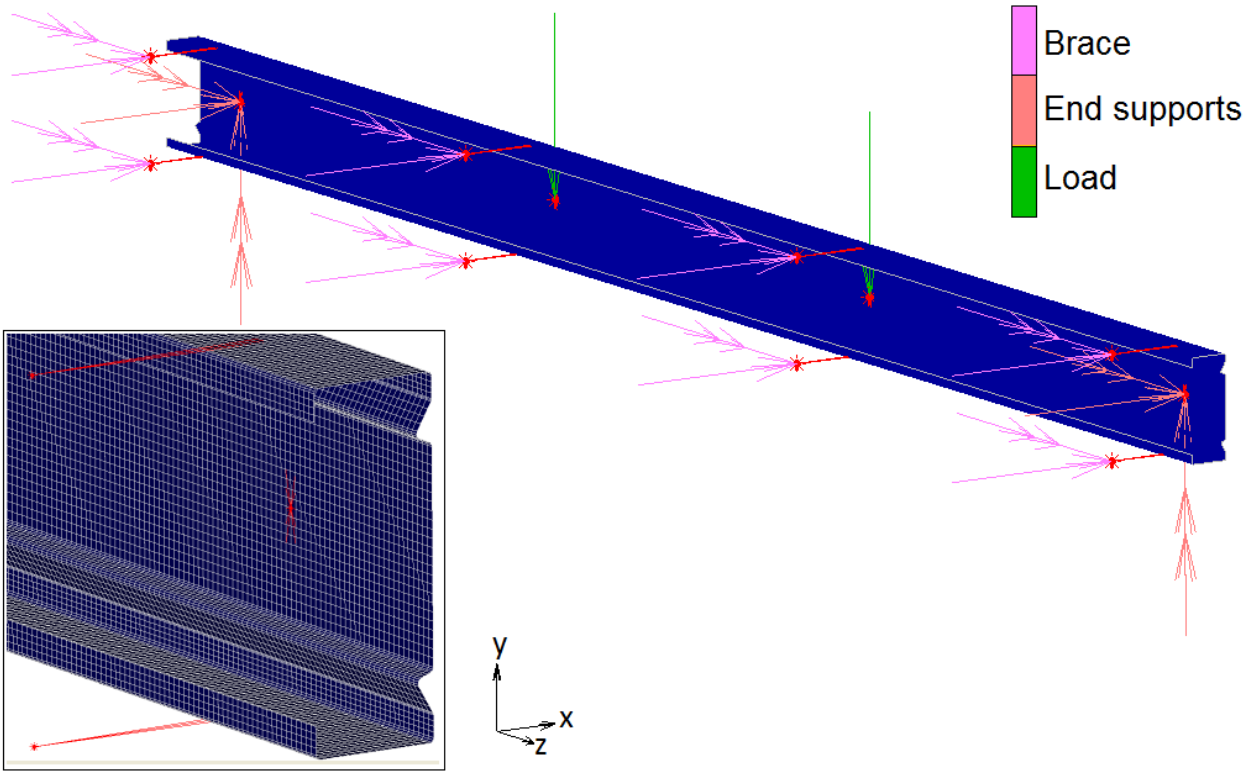

Fig. 3. FEA four-point bending test setup including boundary conditions and a closer view of the mesh of an UltraBEAM^{TM}2

Simulations of the beam test were undertaken in two steps. In the first step, a linear elastic buckling analysis was performed on the perfect beam to obtain its buckling mode shapes (eigenvalues). In the second step, a nonlinear post-buckling analysis was carried out to predict the beam behaviour and ultimate load capacity. The buckling shapes derived in the first step were used as initial geometric imperfections of the beam specimen. In these simulations, the lowest buckling modes were used to generate the imperfections because they are usually the critical buckling modes, and they were similar to the modes obtained from the finite strip analysis software CUFSM and also those observed in tests (for example, FE buckling modes were related to analytical mode in Fig. 4 and compatible with experimental one, as shown in Fig.

6). The degree of initial imperfection was specified as the maximum amplitude of the buckling mode shape and there were several ways to determine it. It was found from previous studies [12, 23] that 0.10t imperfection value produced the best agreement with the test results; therefore, the imperfection value of 0.10t was adopted in this study. In addition, if the consistency of results could be obtained (for beam bending simulations in comparison with tests, as shown in Fig. 5) it could deem to further justify such assumption. Details of FE models were given in Nguyen et al. [12, 23].

5. Test results and discussion

Results of experimental tests, DSM and Finite Element simulations of beam specimens **C-W170T1.6** in the UltraBEAM^{TM}2 test group are presented first. Results of all UltraBEAM^{TM}2 and UltraZED^{TM}2 beams are presented in Table 4.

The results for the elastic buckling analysis using the software CUFSM are provided for the beam specimens **C-W170T1.6** in Fig. 4. The first two minima indicate M_{crl}/M_y = 1.25 and M_{crd}/M_y = 0.75 which clearly shows that the distortional buckling is dominated the behaviour and failure mode of the beams.

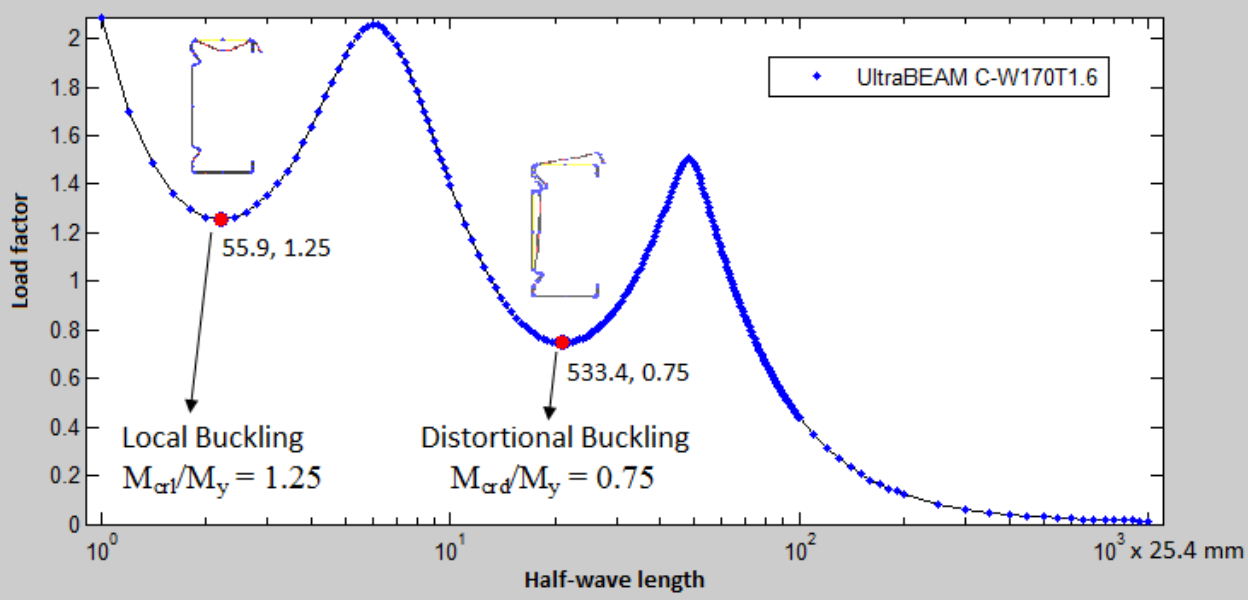

Fig. 4. Buckling curves and modes of the UltraBEAM^{TM}2 specimens **C-W170T1.6** obtained from the software CUFSM [22]. Distortional buckling at the distance of 400 mm between discrete restraints was determined at $M_{crd}/M_y = 0.83$.

Fig. 5 shows the comparison between the experimental, DSM and FE results for the UltraBEAM^{TM}2 specimens. The experimental and FE load-displacement curves were also plotted for comparison. The DSM and FE results were similar in both buckling and ultimate loads, with a maximum difference of less than 9% in buckling load and 6% in ultimate load. The DSM ultimate load was in good agreement with experimental value for ultimate load, with a maximum difference of 12%. However, for this particular example the test did not clearly show elastic buckling prior to failure. It was noted that the buckling loads obtained from the DSM (or more accurate, the finite strip analysis) and FE analysis were even greater than the ultimate

loads. The main reason for this could be the fact that the tested beams deformed in plastic region while the DSM and FE local buckling loads were evaluated by means of linear elastic analysis.

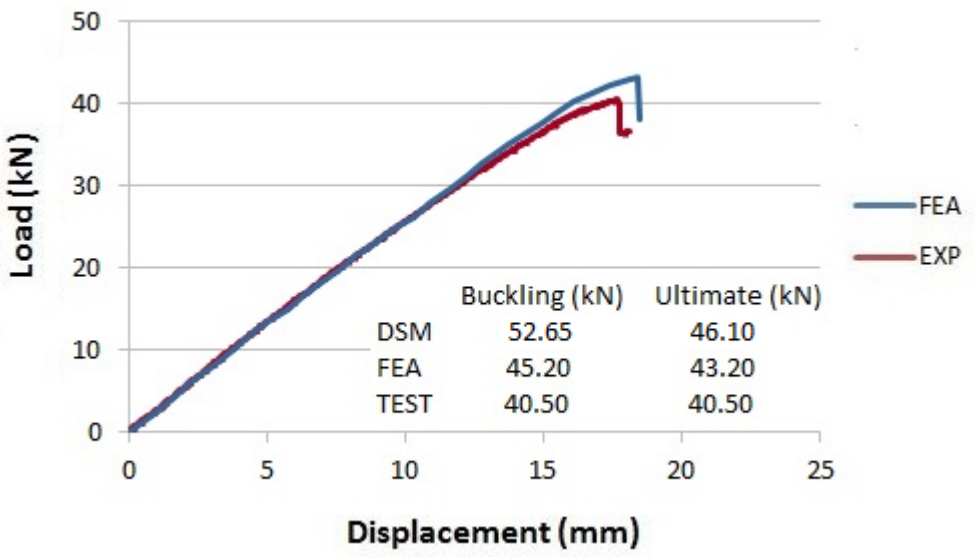

Fig. 5. Results of experimental test, DSM and FE analysis, including load-displacement curves for the UltraBEAM^{TM}2 specimens **C-W170T1.6**

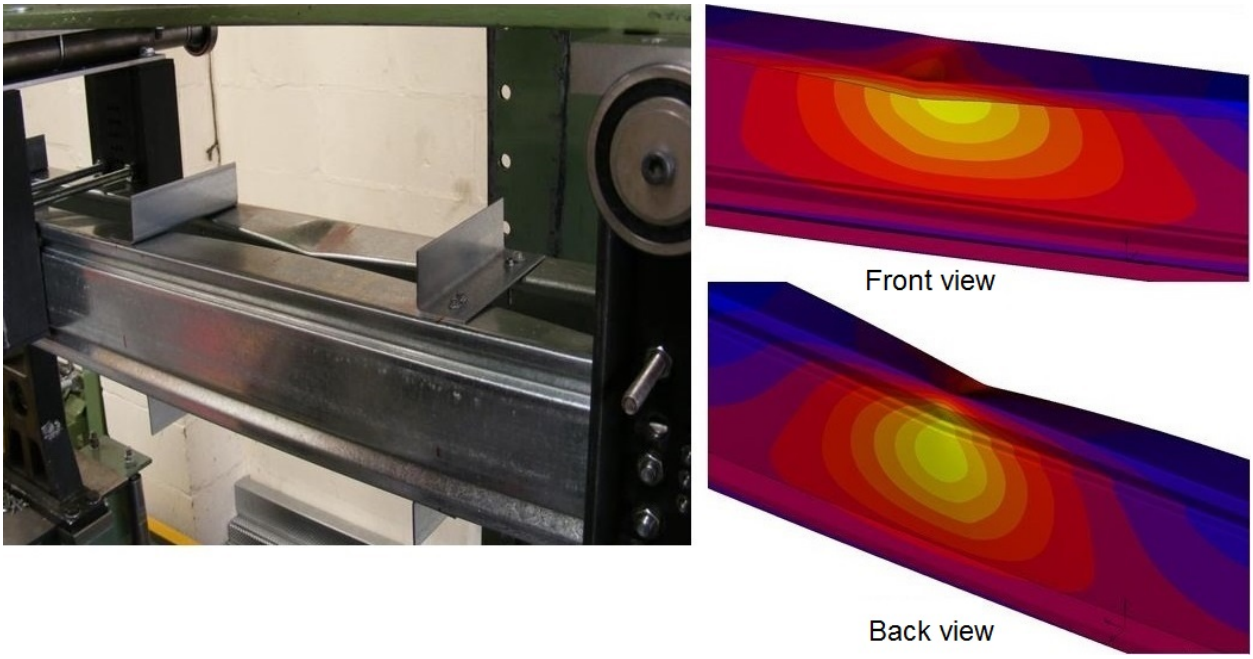

Fig. 6. Failed mode shapes of the UltraBEAM^{TM}2 in testing and FE simulation. Displacement contour is presented in FE results in which lighter colours indicate greater displacement magnitudes

Fig. 6 shows the failed mode shapes of the UltraBEAM^{TM}2 in comparison with the experimental shapes. It can be seen that the buckling and failed modes predicted by DSM and FE models are very similar to the experimental modes. This further confirms the validation of the DSM and FE simulations. Figs. 5 and 6 also show that the beam specimens had similar buckling failure modes in DSM and FE analysis although in DSM the flange modes were assumed to be coming out and the web to be coming in, which are in opposite directions to the experimental and FE analysis modes.

The comparison between the experimental, DSM and FE results for the UltraZED^{TM}2 specimens Z-W170T1.60 is shown in Fig. 7, in which the experimental and FE failure modes were also plotted for comparison. The DSM ultimate load was greater than FE and experimental loads with a maximum difference of 13%. The FE ultimate load was in good agreement with experimental value for ultimate load, with a maximum difference of 7%, and also well captured the failure mode happened in experiment, as illustrated in Fig. 7(b). However, for this test, the zed beam did not clearly show elastic buckling prior to failure, but failed in ‘full section’ mode where it collapsed quickly after plastic yield. The slope of the load-displacement curves, as shown in Fig. 7(a), was almost linear up to the ultimate load indicating the quick collapse of the section which also showed in ‘sharp’ failure shape of the section in Fig. 7(b). This failure mode was different to the buckling failure mode observed with the channel beam presented above where the slope of

the load-displacement curves, as illustrated in Fig. 5, was largely nonlinear up to the ultimate load before failure. These demonstrated the difference between the distortional buckling and full section failure modes.

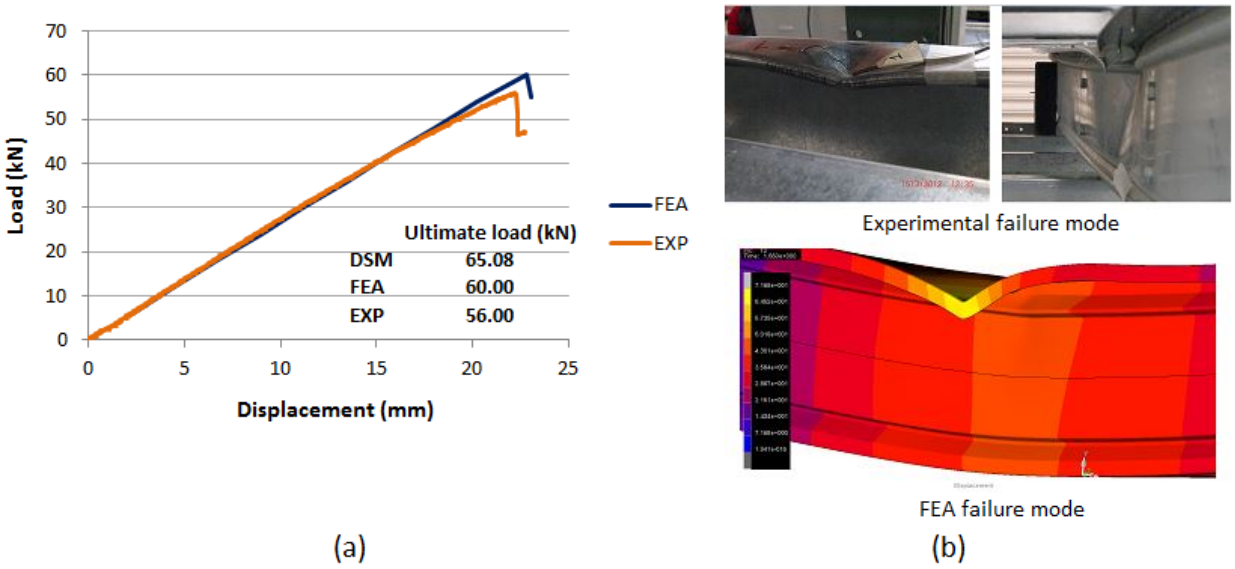

Fig. 7. Results of experimental test, FE analysis and DSM for the UltraZED^{TM}2 specimens **Z-W170T1.6**: (a) load-displacement curves, and (b) failure modes of experiment and FEA

Table 4 Comparison of moment capacities obtained from DSM and test results. 'L', 'D', 'F' stand for 'Local buckling', 'Distortional buckling' and 'Full section', respectively. M_y is yield bending moment on 'Full section'. [a] M_{EXP} is expressed as mean ± SD (Standard Deviation)

Specimens	Test			DSM				Comparison
(1)	M_y (kNm) (2)	[a] M_{EXP} (kNm) (3)	Failure mode (4)	M_{crl} (kNm) (5)	M_{crd} (kNm) (6)	M_{DSM} (kNm) (7)	Failure mode (8)	M_{EXP}/M_{DSM} (9)
UltraBEAM™2								
C-W145T1.2	10.19	5.97 ± 0.38	D	6.23	6.00	6.50	D	0.92
C-W145T1.4	9.41	6.54 ± 0.10	D	9.76	7.68	6.81	D	0.96
C-W145T2.0	13.20	11.24 ± 0.37	D	27.57	14.77	10.72	D	1.05
C-W170T1.2	12.47	6.63 ± 0.23	D	7.68	7.03	7.82	D	0.85
C-W170T1.5	14.27	8.43 ± 0.14	D	14.74	10.05	9.77	D	0.86
C-W170T1.6	14.17	9.08 ± 0.16	D	17.80	11.80	10.34	D	0.88
C-W170T2.0	17.25	12.75 ± 0.51	D	32.60	16.31	13.19	D	0.97
C-W255T1.5	19.36	13.21 ± 0.37	D	26.27	17.63	14.60	D	0.90
C-W255T2.3	30.48	23.82 ± 0.33	D	91.71	36.27	25.27	D	0.94
C-W255T3.0	42.43	40.09 ± 1.21	D	198.06	61.95	37.64	D	1.07
UltraZED™2								
Z-W145T1.2	7.53	7.29 ± 0.25	F	15.41	25.29	7.53	F	0.97
Z-W145T1.5	9.97	9.50 ± 0.10	F	29.49	40.21	9.97	F	0.95
Z-W145T2.0	13.68	12.35 ± 0.29	F	68.38	73.54	13.68	F	0.90
Z-W170T1.6	14.35	12.54 ± 1.30	F	65.40	49.23	14.35	F	0.87
Z-W200T1.2	15.31	10.75 ± 0.23	F	28.74	29.72	14.80	F	0.73
Z-W200T1.8	20.56	17.19 ± 0.26	F	91.42	68.81	20.56	F	0.84
Z-W200T2.5	23.83	22.20 ± 0.36	F	219.76	135.65	23.84	F	0.93
Z-W255T1.3	18.46	16.50 ± 0.28	L	27.46	29.98	16.93	L	0.97
Z-W255T1.8	26.09	25.18 ± 0.10	F	67.25	58.90	26.09	F	0.97
Z-W255T2.5	32.86	31.98 ± 0.24	F	173.75	115.15	32.86	F	0.97

Table 4 shows the results of ultimate moment capacities of all UltraBEAM^{TM}2 and UltraZED^{TM}2 beams obtained from experimental test (M_{EXP}) and Direct Strength Method (M_{DSM}). In Table 4, the experimental results M_{EXP} was expressed as mean ± SD (Standard Deviation). 'Full section' failure mode indicates the beam fails at yield stress or the full cross section is effective under loads. The comparison between these values is shown in column (9) of Table 4. Comparison of the DSM results with experimental test results shows a minimum variation of 3% up to a maximum of 15% for channel sections, and 3% to 16% for zed sections with only an abnormal maximum of 27%, being one out of 20 data. The average variation in bending moment achieved through the DSM and physical testing is 8% and 10% for all data of channel and zed sections, respectively, with the DSM giving less conservative results in 2/20 cases. The average deviation in the test results for channel and zed beams were ±0.28 and ±0.23, respectively, indicating test results had small errors and good agreements with DSM results, as shown in Table 4. In addition, the modes of failure observed during experimental tests were similar with those obtained from the DSM calculations, as shown in columns (3) and (5). In experimental tests of UltraBEAM^{TM}2 specimens, it was observed that as the load increased, wavelike deflections appeared along the length of the flanges and of the beam specimens, and the flange edges bent down; these beam specimens clearly exhibited 'distortional buckling'. However, for many UltraBEAM^{TM}2 beams, this phenomenon happened fast and followed by failure of the beams. These show a very good agreement between test and DSM design values. Many UltraZED^{TM}2 specimens failed at yield bending moment so their cross sections were fully effective or under 'Full section' failure mode whilst beams with depths of 145 mm did not show buckling failure clearly so they were also defined as 'Full section' failure.

Trends have been identified between bending moment capacity and depth-to-thickness ratio for a range of UltraBEAM^{TM}2 and UltraZED^{TM}2 beams from both experimental and DSM results. A decrease in depth-to-thickness ratio shows an increase to bending moment capacity for the given depth-to-thickness range. This has been shown for the UltraBEAM^{TM}2 and UltraZED^{TM}2 sections in columns (2) and (4), respectively.

The results of DSM using a distortional buckling at a half-wave length were rationally evaluated by comparing them with FEA and experimental results. For example, the DSM and FEA results of the specimen C-W170T1.6 were in excellent agreement in both buckling and ultimate load as shown in Fig. 5. The DSM half-wave length for distortional buckling was 533.4 mm which was compatible to the buckling length of approximate 550 mm as observed from the test and FEA simulation. The DSM results were also in good agreement with the experimental results as shown in Table 4. The comparison indicated that the DSM results are more conservative than experimental ones with an average variation of 6-10%. These could deem to further justify the use of DSM for the UltraBEAM^{TM}2 and UltraZED^{TM}2 sections tested in this study by using a distortional buckling stress at the distance between discrete restraints that limited the distortional buckling.

Table 5 Failure modes identified from DSM for 305 mm deep UltraZED^{TM}2 range

Section Depth	Thickness	Bending Moment	Depth-to-thickness Ratio	Failure Mode	Reduction in capacity
(mm)	(mm)	(kNm)			(%)
305	1.50	22.34	203.33	Distortional Buckling	-13%
305	1.60	24.32	190.63	Distortional Buckling	-11%
305	1.80	28.35	169.44	Distortional Buckling	-8%
305	2.00	32.51	152.50	Distortional Buckling	-4%
305	2.30	38.80	132.61	Full section capacity	0%
305	2.50	42.01	122.00	Full section capacity	0%
305	3.00	49.92	101.67	Full section capacity	0%

The depth-to-thickness ratio shows a relationship between the exhibited failure modes within a section range. Sections with the lowest depth-to-thickness ratio show a fully effective section capacity, while the higher depth-to-thickness ratios show a reduced section capacity caused by local and distortional buckling effects. Where buckling effects are dominant the effective section modulus will be used to calculate the moment capacity. Where the full section capacity is dominant the gross section modulus will be used to calculate the section capacity. This has been shown for the 305mm deep zed profile range in Table 5. Observations from Table 5 show that

sections with a higher depth-to-thickness ratio exhibited greater effects from buckling than sections with a lower depth-to-thickness ratio. The magnitude of capacity reduction generated from buckling effects is between 0% and 13% for UltraZED^{TM}2 sections, and between 5% and 37% for UltraBEAM^{TM}2 sections.

6. Conclusions

The experimental test and design by the Direct Strength Method for the new channel and zed purlins with web longitudinal stiffeners namely UltraBEAM^{TM}2 and UltraZED^{TM}2 were presented. Simply supported UltraBEAM^{TM}2 and UltraZED^{TM}2 beams were tested under four-point bending about the major axis of the sections. In addition to experimental tests, a non-linear Finite Element model was developed and verified against the test results. The DSM was first evaluated by comparing its predicted bending moment capacities with those of test and Finite Element analysis for a four-point bending test of UltraBEAM^{TM}2 and UltraZED^{TM}2 sections. The comparison shows excellent agreements between the DSM, test and Finite Element results, including failed modes. Based on this validation, the DSM was used to predict the bending strength of a wide range of UltraBEAM^{TM}2 and UltraZED^{TM}2 sections and results were compared with test results. A total of 20 different purlin sections including 10 specimens of UltraBEAM^{TM}2 and 10 UltraZED^{TM}2 sections were investigated. Each section with the same depth had three different thicknesses that ranged from 1.20 mm to 3.05 mm in order to cover a wide popular range of section slenderness used in building construction. The overall beam depth-to-thickness ratios were studied. Four duplicated tests were carried out for each section so there were 116 tests in total for both UltraBEAM^{TM}2 and UltraZED^{TM}2 purlins.

Comparison of the DSM results with physical test results shows an average variation of 8% for the UltraBEAM^{TM}2 sections and 10% for the UltraZED^{TM}2 sections, with the DSM giving conservative results in 2/20 cases. This shows that the nominal moment capacities predicted using the DSM are very comparable with test results for the UltraBEAM^{TM}2 and UltraZED^{TM}2 purlins subjected to bending. Therefore, it is recommended that the current Direct Strength Method in the North American Standard [2,3] can be used for the strength design of cold roll formed UltraBEAM^{TM}2 and UltraZED^{TM}2 purlins subjected to bending.

The experimental results presented in this study represent the bending tests of the new cold roll formed UltraBEAM^{TM}2 and UltraZED^{TM}2 sections with particular geometries and slenderness that are widely used in the building construction. It was observed that the distortional buckling dominated the behaviour and failure mode of all the UltraBEAM^{TM}2 sections whilst it occurred only in few UltraZED^{TM}2 sections; most of UltraZED^{TM}2 sections behaved elastically in full strength without buckling. Therefore, these results might not be sufficient to make a definitive guide of using the DSM to a large number of UltraZED^{TM}2 sections that are available. However, the results of this study can be used as a basic for suggesting the implementation of the DSM for the design of such sections.

On-going work includes an extended testing program and the use of the DSM for the UltraBEAM^{TM}2 and UltraZED^{TM}2 sections taking into account local buckling and especially distortional buckling for UltraZED^{TM}2 sections together with shear behaviour. This involves the use of Finite Element analysis and further experimental validation.

References

[1] BS EN 1993-1-3:2006. Eurocode 3 – Design of steel structures. Part 1-3: General rules – Supplementary rules for cold-formed members and sheeting.

[2] AISI S100-2012. North American Specification for the Design of Cold-Formed Steel Structural Members. 2012 Edition. American Iron and Steel Institute, Washington, D.C.

[3] AISI 2005. Supplement 2004 to the North American specification for the design of cold-formed steel structural members. 2001 Edition. American Iron and Steel Institute, Washington, D.C.

[4] AS/NZS 4600:2005. Australian/New Zealand standard cold-formed steel structures.

[5] Desmond TP, Pekoz T, Winter G. Local and overall buckling of cold formed compression members. Department of Structural Engineering Report, Cornell University 1978.

[6] Papazian RP, Schuster RM, Sommerstein M. Multiple stiffened deck profiles. Proceedings of the 12th International Specialty Conference on Cold-Formed Steel Structures 1994;217-228.

[7] Schafer BW, Peköz T. The behaviour and design of longitudinally stiffened thin-walled compression elements. Thin-Walled Structures 1998;27:65-87.

[8] Young B, Chen J. Design of cold-formed steel built-up closed sections with intermediate stiffners. Journal of Structural Engineering 2008;134:727-737.

[9] Zhang JH, Young B. Compression tests of cold-formed steel I-shaped open sections with edge and web stiffeners. Thin-Walled Structures 2012;52:1-11.

[10] Rhodes J, Zaras J. Development and design analysis of a new purlin system. Proceedings of the 9th International Specialty Conference on Cold-Formed Steel Structures 1988;215-228.

[11] Castellucci MA, Pillinger I, Hartley P, Deeley GT. The optimisation of cold rolled formed products. Thin-Walled Structures 1998;1-4:159-174.

[12] Nguyen VB, English MA, Castellucci MA. FE simulation techniques for new process and product developments in metal forming industry. Proceedings of the 13th International Cold Forming Congress 2015;178-185.

[13] Schafer BW, Peköz T. Direct strength prediction of cold formed steel members using numerical elastic buckling solutions. Thin-Walled Structures, Research and Development. Proceedings of the 18th International Specialty Conference on Cold-Formed Steel Structures 1998; 69-76.

[14] Yu C, Schafer, BW. Local buckling tests on cold-formed steel beams. Journal of Structural Engineering 2003;129:1596-1606.

[15] Yu, C, Schafer, BW. Distortional buckling tests on cold-formed steel members in bending. Journal of Structural Engineering 2006;132:515-528.

[16] Javaroni CE, Goncalves RM. Distortional buckling of simple lipped channel in bending results of the experimental analysis versus direct strength methods. Proceedings of the 18th International Specialty Conference on Cold-Formed Steel Structures 2006;133-146.

[17] Pham CH, Hancock GJ. Experimental investigation and Direct Strength Design of high-strength, complex C-sections in pure bending. Journal of Structural Engineering 2013; 10:1842-1852.

[18] Schafer BW. Designing cold-formed steel using the direct strength method. Proceedings of the 18th International Specialty Conference on Cold-Formed Steel Structures 2006; October 26-27, 2006, Orlando, Florida, USA.

[19] BS EN 10002-1:2001. Metallic materials - Tensile testing - Part 1: Method of test at ambient temperature.

[20] Nguyen VB, Wang CJ, Mynors DJ, English MA, Castellucci MA. Compression tests of cold-formed plain and dimpled steel columns. Journal of Constructional Steel Research 2012;69:20-29.

[21] Schafer BW, Adany S. Buckling analysis of cold-formed steel members using CUFSM: conventional and constrained finite strip methods. Proceedings of the 18th International Specialty Conference on Cold-Formed Steel Structures 2006;39-54.

[22] CUFSM, version 4.05; 2012. URL: http://www.ce.jhu.edu/bschafer/cufsm/ (latest updated on 24th May 2012).

[23] Nguyen VB, Wood PKC, English MA, Castellucci MA. The design and development of new cold roll formed products by finite element modelling and optimisation. Accepted for publication in the Proceedings of the 23rd International Specialty Conference on Cold-Formed Steel Structures 2016; November 9-10, 2016, Baltimore, Maryland, USA.